Doped Nanocrystals

DOI: 10.1002/anie.201105025

Sodium Doping Controlled Synthesis of Monodisperse Lanthanide Oxysulfide Ultrathin Nanoplates Guided by Density Functional Calculations**

Yi Ding, Jun Gu, Jun Ke, Ya-Wen Zhang, and Chun-Hua Yan**

Doping of nanocrystals is an intriguing field, since the intentional introduction of impurities has long been regarded as a major way of tailoring the properties of materials. Furthermore, it was recently found that the use of dopants in the synthesis of inorganic colloidal nanocrystals can not only introduce novel properties but also influence shape and size evolution during nanocrystal nucleation and growth.[1] For example, Liu and co-workers showed that $NaYF_4$-based nanocrystals can be precisely tuned in size, phase, and upconversion emission through Gd^{3+} doping.[1d] Wang and co-workers reported that lanthanide doping of alkaline earth metal fluoride nanocrystals can lead to a significant increase in monodispersity.[1h]

On the other hand, the special 4f electron configurations of lanthanides endow their compounds with promising functionalities, such as luminescence, catalytic activity, and permanent magnetism.[2] This has therefore stimulated recent efforts to synthesize colloidal lanthanide-based nanocrystals (Ln-based NCs) with tunable morphologies and unique material properties.[3] For example, both the small size and excellent luminescence properties make Ln-based NCs a potential new type of fluorescent probes.[2a,3a] Specifically, lanthanide oxysulfides (Ln_2O_2S; Ln = La, Gd, Y) can serve as one of the most effective hosts for fluorescence applications, and research on Ln_2O_2S NCs is therefore highly intriguing.[4] However, the synthesis of monodisperse Ln_2O_2S NCs remains a challenge, since the theory of hard and soft acids and bases (HSAB)[5] predicts a lack of affinity between the hard Lewis acid Ln^{3+} and the soft Lewis base S^{2-}. Previously, Gao and co-workers presented pioneering work in the synthesis of monodisperse lanthanide oxysulfide nanocrystals, yet due to the difficulty in preparing the corresponding single-source precursors, this method was limited to only a few lanthanides (i.e., Sm, Eu, Gd).[4a]

On the basis of both experimental characterization and DFT calculations, we now demonstrate that introduction of monovalent Na^+ ions as dopants in trivalent Ln^{3+} host lattices can significantly facilitate the formation of Ln_2O_2S NCs in oleic acid (OA)/oleylamine (OM)/1-octadecene (ODE) mixed solvent by creating oxygen vacancies in the host lattice during sulfurization reactions.

In a typical synthesis, monodisperse and single-crystalline Na-doped La_2O_2S nanoplates were formed with a diameter of (22.3 ± 2.0) nm (Figure 1a and b). High-resolution transmission electron microscopy (HRTEM) revealed that the morphology of the as-synthesized nanoplates was mainly hexagons with six {100} facets as their side planes (Figure 1b). When the dispersion of nanoplates in cyclohexane was highly

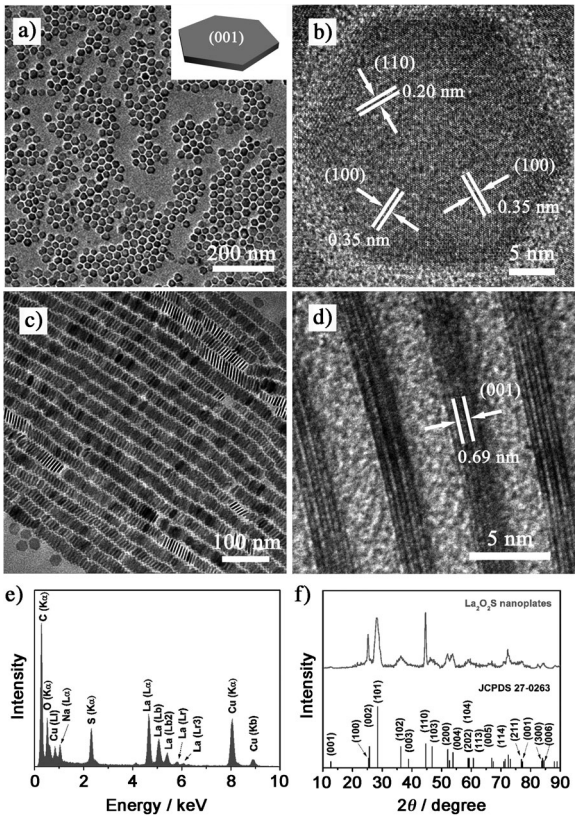

Figure 1. a) TEM and b) HRTEM (taken with [001] incidence) images of Na-doped La_2O_2S nanoplates. c) TEM and d) HRTEM (taken with [100] incidence) images of the nanoplate superlattice. e) EDS spectrum of the nanoplates. f) WAXRD pattern of the nanoplates.

[*] Y. Ding, J. Gu, J. Ke, Prof. Y.-W. Zhang, Prof. C.-H. Yan
Beijing National Laboratory for Molecular Science, State Key Laboratory of Rare Earth Materials Chemistry and Applications
PKU-HKU Joint Laboratory in Rare Earth Materials and Bioinorganic Chemistry, College of Chemistry and Molecular Engineering
Peking University, Beijing 100871 China
E-mail: ywzhang@pku.edu.cn
yan@pku.edu.cn

[**] This work was supported by the NSFC (grant nos. 21025101, 20871006, and 20221101). Y.W.Z. particularly appreciates the financial aid of China National Funds for Distinguished Young Scientists from the NSFC. The authors also acknowledge the help in theoretical calculation from Dr. Jun Jiang and Dr. Rui Qin of Peking University.

Supporting information for this article is available on the WWW under http://dx.doi.org/10.1002/anie.201105025.

concentrated, evaporation-induced self-assembly could generate nanoplates arrays with face-to-face orientation (Figure 1c and d). The HRTEM image of the nanoplates lying on their side planes showed that they were bound by two {001} facets and comprised only three layers of crystal cells along the *c* axis (Figure 1d; (2.1 ± 0.2) nm in thickness). Energy-dispersive X-ray analysis (EDS) and wide-angle X-ray diffraction (WAXRD) also demonstrated formation of Na-doped La_2O_2S NCs (Figure 1e and f and Supporting Information, Table S1) in a hexagonal structure (JCPDS 27-0263). Incorporation of Na^+ ions into the La_2O_2S host lattice was further confirmed by X-ray photoelectron spectroscopy (XPS) and inductively coupled plasma atomic emission spectroscopy (ICP-AES; Supporting Information, Table S1). The average of the molar Na:La ratios determined by the three methods is 21:79%.

Sodium-doping-induced competition between La_2O_2S and La_2O_3 seems to play a key role in the formation of Na-doped La_2O_2S NCs. When only $La(acac)_3$ (acac = acetylacetonate) was utilized as precursor, the product was La_2O_3 NCs. When both $La(acac)_3$ and sulfur powder (S) were used as the precursors, only nanowires (NWs) with sub-1 nm thickness (oil-like sample) were obtained (Supporting Information, Figure S1a,b). The absence of both HRTEM lattice fringes (Supporting Information, Figure S1c) and XRD peaks for the NWs indicated formation of organic–inorganic composites. Interestingly, however, on introduction of a certain amount of Na^+ ions, that is, when $La(acac)_3$, Na(acac), and S were added simultaneously as precursors, ultrathin nanoplates were produced in the hexagonal phase of La_2O_2S (Supporting Information, Figure S1d–f). With only $La(acac)_3$ and Na(acac) as precursors, La_2O_3 NCs containing about 10% Na species (much lower than that in the as-synthesized Na-doped La_2O_2S NCs) were obtained (see Supporting Information, Table S1 and Figure S2).

To elucidate the function of Na^+ doping in La_2O_2S and to guide the synthesis, we performed DFT calculations (for details, see Supporting Information). The monomers of each constituent element X (X = La, O, S, Na) in solution can be described by its chemical potential μ_X. The thermodynamic requirements for crystal formation include: 1) μ_X is bound by the chemical potentials of the elementary substances, that is, when μ_X is set to 0 in their respective most stable elemental form, it is required that $\mu_X < 0$ in solution, otherwise elemental substance would form. 2) To maintain a stable La_2O_2S compound, it is required that [Eq. (1)].

$$2\mu_{La} + 2\mu_O + \mu_S = \mu_{La_2O_2S} \quad (1)$$

3) $\mu_{La_2O_2S}$ is also bound by other competitive compounds (e.g., La_2O_3 and La_2S_3, since these are the most common oxide and sulfide of lanthanum, respectively), so the chemical potential of the monomers in solution should also satisfy the following relationships [Eqs. (2a) and (2b)].

$$2\mu_{La} + 3\mu_O < \mu_{La_2O_3} \quad (2a)$$

$$2\mu_{La} + 3\mu_S < \mu_{La_2S_3} \quad (2b)$$

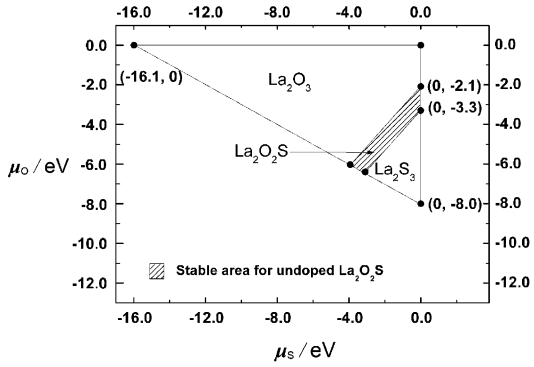

Figure 2. Calculated phase diagram with respect to chemical potential of O (μ_O) and S (μ_S).

The aforementioned requirements can thus be utilized to illustrate the stable area for La_2O_2S with respect to μ_O and μ_S with La_2O_3 and La_2S_3 as constraints (Figure 2).

The relatively high doping concentration of Na^+ in the La_2O_2S lattice suggests that the growth mechanism of the nanoplates should be governed by the trapped-dopant model.[1a,b] Once doped in the La_2O_2S host, the Na^+ ions would occupy the La^{3+} sites, forming $Na_{La}^{\times\times}$ defects. Since the ionic radius of Na^+ (r_{Na^+} = 1.02 Å) is very close to that of La^{3+} ($r_{La^{3+}}$ = 1.03 Å),[6] Na doping leads to a small shift towards lower angle in the XRD pattern (Supporting Information, Table S3) that results from an expansion of the unit cell by about 1% along the *c* axis, possibly due to decreased Coulomb interactions in the lattice. After formation of $Na_{La}^{\times\times}$, two possible anion vacancies $V_O^{\bullet\bullet}$ and $V_S^{\bullet\bullet}$ could be generated to maintain the charge balance. The supercell model[7] is therefore used to calculate the formation energy of $V_O^{\bullet\bullet}$ and $V_S^{\bullet\bullet}$, and to further determine which kind of vacancy would form. The supercell used in our calculation contained $2 \times 2 \times 1$ repetition of the primitive unit cell with one La atom replaced by Na (Figure 3).

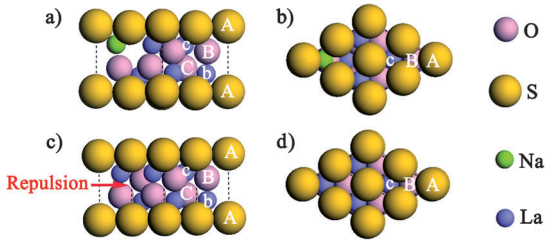

Figure 3. Calculated $2 \times 2 \times 1$ supercell of Na-doped La_2O_2S seen in a) ⟨110⟩ and b) ⟨001⟩ directions. Calculated $2 \times 2 \times 1$ supercell of undoped La_2O_2S seen in c) ⟨110⟩ and d) ⟨001⟩ directions.

According to Figure 2, formation of La_2O_2S dictates the relationship in Equation (3), and the difference in formation energy between $V_O^{\bullet\bullet}$ and $V_S^{\bullet\bullet}$ on doping with Na^+ can be written as Equation (4).

$$-3.3\ \text{eV} \le \mu_O - \mu_S \le -2.1\ \text{eV} \qquad (-4.37\ \text{eV} \le \mu_S \le 0) \quad (3)$$

$$H_f(V_O^{\bullet\bullet}) - H_f(V_S^{\bullet\bullet}) = E_{La_2O_2SwithV_O^{\bullet\bullet}andNa_{La}^{\times}} - E_{La_2O_2SwithV_S^{\bullet\bullet}andNa_{La}^{\times}} + \mu_O - \mu_S = 2.0\,eV + \mu_O - \mu_S \quad (4)$$

Thus, the difference in formation energy of $V_O^{\bullet\bullet}$ and $V_S^{\bullet\bullet}$ can be plotted against the difference of μ_O and μ_S (Figure 4a). Since the formation energy of $V_O^{\bullet\bullet}$ is always smaller than that of $V_S^{\bullet\bullet}$, $V_O^{\bullet\bullet}$ is the dominant anion vacancy on doping with Na^+. The formation of $V_O^{\bullet\bullet}$ was also corroborated by elemental analysis (Supporting Information, Table S1).

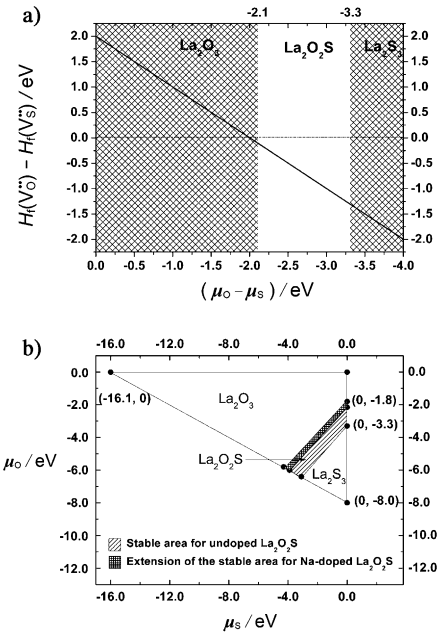

Figure 4. a) Calculated difference in vacancy-formation energy $\left[H_f(V_O^{\bullet\bullet}) - H_f(V_S^{\bullet\bullet})\right]$ versus difference in chemical potential. b) Calculated phase diagram for undoped and doped compounds with respect to chemical potential of O (μ_O) and S(μ_S).

The doping-induced composition control can be further elucidated by the calculated phase diagram after Na doping (Figure 4b). Since La_2S_3 NCs have not been synthesized in OA/OM/ODE mixed solvent to the best of our knowledge, and the affinity between La and O is higher than that between La and S, formation of La_2O_2S is mainly competitive with formation of La_2O_3, and the La_2S_3 phase is shown in the diagram only as a constraint for the stable area of La_2O_2S. The calculated composition diagram with respect to μ_S and μ_O demonstrates the relationship between La_2O_2S and La_2O_3: doping with Na^+ can greatly increase the stable area of La_2O_2S, so that the formation of La_2O_2S can tolerate lower μ_S and higher μ_O (OA as both capping agent and solvent generally causes high μ_O), which is in good agreement with our experimental results. Formation of the La_2O_2S phase can therefore be viewed as the following process: when Na^+ ions are doped in the NCs, they reduce the amount of O^{2-} in the crystals to a certain extent, so that formation of La_2O_2S is preferable. Besides calculations, further structural examination of the function of Na^+ doping is also illustrated in Figure 3. The crystal structure of La_2O_2S can be described as |AcBCb| AcBCb type along the ⟨001⟩ direction (Figure 3c and d), where uppercase A represents one layer of hexagonal close packed (hcp) S^{2-}; uppercase B and C represent one layer of hcp O^{2-}, respectively; and lowercase b and c represent one layer of hcp La^{3+}. As La_2O_2S has only two cations and three anions in the primitive cell, repulsion between two O^{2-} layers can be regarded as the major cause of the instability of the La_2O_2S phase (Figure 3c). Introduction of Na^+ generates $V_O^{\bullet\bullet}$ and thus markedly reduces the repulsion and leads to formation of Na-doped La_2O_2S NCs. Formation of $V_O^{\bullet\bullet}$ is also indicated by the XPS analysis (Figure S3, Supporting Information). The determined molar ratio of O:La of 0.72 is lower than that of bulk La_2O_2S (0.93).

Besides doping-induced composition control, we also observed several interesting self-assembly phenomena of the as-synthesized nanoplates. Specifically, when the amount of OA was increased from 2.5 to 5 mmol while maintaining the quantities of the other precursors and solvents, the nanocrystals could self-assemble by face-to-face packing into long fiberlike NWs with lengths of several micrometers (Figure 5a, top-right inset), and the as-formed NWs could further intertwine into bundles of arrays. (Figure 5b). Interestingly, the NWs are formed during the synthetic process above 300 °C, since the reaction solution turned milky within 10 min and remained without phase separation for a prolonged reaction time. Both small-angle XRD (Supporting Information, Figure S5) and HRTEM measurements indi-

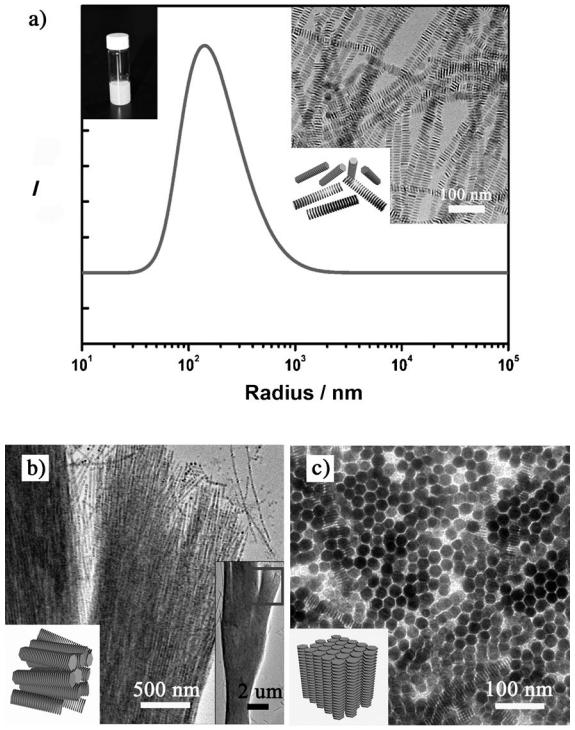

Figure 5. a) DLS characterization of nanoplates dispersed in cyclohexane (top left: photograph of the nanoplate dispersion; top right: TEM image of the fiberlike primary superlattice of nanoplates ($(2.6\pm0.3)\times(23.0\pm3.5)$ nm). b) TEM images of the bundlelike secondary superlattice of nanoplates parallel to the copper grid (bottom right: low-magnification TEM image). c) TEM image of hcp NW arrays perpendicular to the copper grid.

cated that the interplate distance of two neighboring nanoplates is about 3.0 nm, nearly twice the length of the carbon chain of OA or OM. These results strongly suggest that the interchain molecular interaction of the capping agents were strong enough to sustain thermal fluctuation at above 300 °C. The as-synthesized nanoplates remain assembled after post-synthesis procedures, since strong opalescence could be observed when the nanoplates were dispersed in nonpolar solvents (Figure 5a, top-left inset). This assumption was also confirmed by dynamic light scattering (DLS) experiments (Figure 5a) with a peak value at 180 nm. We can therefore make further use of these NWs formed in solution by performing a self-assembly process at the liquid/air interface.[8] The NWs can be dragged perpendicular to the interface when subjected to evaporation, and thus form a secondary superlattice of hexagonal close packed, perpendicularly aligned NW arrays (Figure 5c and Supporting Information, S7).

Using the present doping method, we can also obtain different kinds of ultrathin Ln_2O_2S nanoplates of hexagonal phase (Ln = Pr–Tb; Supporting Information, Figures S8 and S9). The gradual mismatch of the radii between Na^+ and Ln^{3+} makes the doping process more difficult when Ln^{3+} gets heavier. However when Li(acac) is utilized, Y_2O_2S NCs can also be synthesized (Supporting Information, Figure S10). Further doping with Eu or Tb (Supporting Information, Figures S11 and S12, Table S2) can produce La_2O_2S:4% Eu nanoplates ($(2.1 \pm 0.2) \times (25.5 \pm 3.5)$ nm) and La_2O_2S:1% Tb nanoplates ($(2.4 \pm 0.4) \times (27.5 \pm 4.5)$ nm) in hexagonal structure, which show intense red and green fluorescence, respectively (Figure 6). With excitation at 340 nm, the photoluminescence quantum yield (PLQY) was determined to be 4.3% for the Na-doped La_2O_2S:4% Eu NCs, which is lower than that of bulk La_2O_2S:4% Eu (38.2%). The fluorescence of Eu^{3+} in the La_2O_2S lattice is ascribed to the transitions from $^5D_0$ to ^7F_J ($J = 0$–2, 4), while the fluorescence of Tb^{3+} is ascribed to transitions from $^5D_4$ to ^7F_J ($J = 3$–6).[4] The fluorescence colors of Eu^{3+} and Tb^{3+} in La_2O_2S can be described on the *xy* chromaticity diagram as (0.58, 0.40) and (0.32, 0.54), respectively, while the corresponding bulk materials have (0.64, 0.35) and (0.32, 0.60). Specifically, the fluorescence of Eu^{3+} can also serve as an indicator of Na doping in La_2O_2S NCs. The ratio between $^5D_0$ to $^7F_1$ and $^5D_0$ to $^7F_4$ intensity (I_1/I_4) indicates the long-range effect related to bulk La_2O_2S, whereas the ratio between $^5D_0$ to $^7F_1$ and $^5D_0$ to $^7F_2$ intensity (I_1/I_2) indicates the local structure changes in vicinity of the Eu^{3+} ion.[9] Since Na^+ doping could lead to O^{2-} vacancies near Na^+ sites, the vicinity of Eu^{3+} remains almost intact, and very little changes in I_1/I_2 ratio occur, whereas the long-range interaction changes, and thus the I_1/I_4 ratio of nanoplates is distinctly lower than that of the bulk material. Figure S13b and Figure S14b of the Supporting Information show the luminescence decay curves of La_2O_2S:Eu NCs (623 nm emission of Eu^{3+}) and La_2O_2S:Tb NCs (544 nm emission of Tb^{3+}), respectively, which can be fitted into a single-exponential function [Eq. (5)]

$$I = I_0 e^{-\frac{t}{\tau}} \quad (5)$$

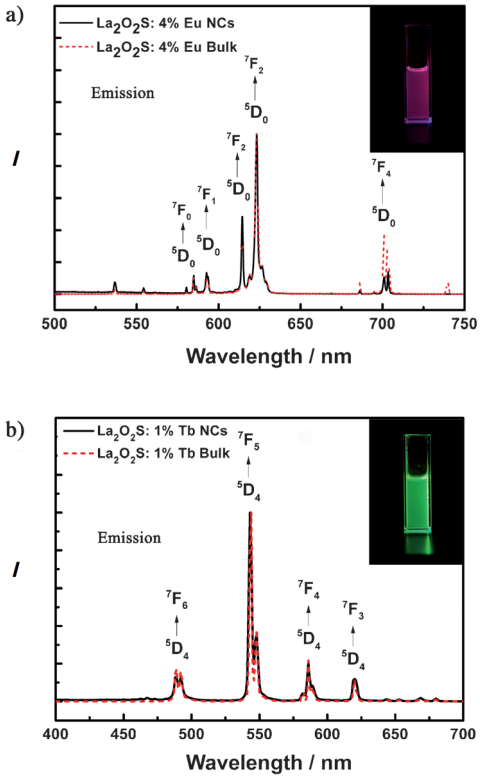

Figure 6. a) Emission spectrum of Na-doped La_2O_2S: 4% Eu nanoplates and its bulk counterpart at $\lambda_{ex} = 340$ nm. b) Emission spectrum of Na-doped La_2O_2S:1% Tb nanoplates and its bulk counterpart under $\lambda_{ex} = 300$ nm. The insets of a) and b) are photographs of Na-doped La_2O_2S:4%Eu NCs and Na-doped La_2O_2S:1% Tb NCs dispersed in cyclohexane and excited with a UV lamp at 365 nm, respectively.

where for La_2O_2S:Eu, τ is 640 μs for nanoplates and 340 μs for bulk material; and for La_2O_2S:Tb, τ is 1221 μs for nanoplates and 637 μs for bulk material. The luminescence lifetimes of both La_2O_2S:Eu NCs and La_2O_2S:Tb NCs are longer for nanoplates than for their bulk counterparts, possibly due to the decreased radiative transition rate originating from the change in effective refractive index on Na doping in La_2O_2S.[4c,10]

In summary, both theoretically and experimentally, we have demonstrated that doping with Na^+ ions could lead to the syntheses of monodisperse sub-2 nm-thick Ln_2O_2S nanoplates with tunable self-assembly patterns and robust fluorescence through formation of oxygen vacancies during sulfurization reaction in solution. The nanoplates can form NW-like superstructures and even higher-ordered superstructures, such as bundlelike nanoarrays and hcp, perpendicularly aligned nanoarrays. This combined theoretical and experimental method can provide new insights into the solution chemistry of nanocrystal synthesis, and the present doping strategy of composition control at the nanoscale may also be applicable to the syntheses of many other doped inorganic NCs with unique material properties.

Received: July 18, 2011
Revised: September 1, 2011
Published online: October 21, 2011

Keywords: density functional calculations · doping · lanthanides · nanoparticles · phase diagrams

[1] a) M. H. Du, S. C. Erwin, A. L. Efros, *Nano Lett.* **2008**, *8*, 2878; b) S. C. Erwin, L. J. Zu, M. I. Haftel, A. L. Efros, T. A. Kennedy, D. J. Norris, *Nature* **2005**, *436*, 91; c) D. J. Norris, A. L. Efros, S. C. Erwin, *Science* **2008**, *319*, 1776; d) F. Wang, Y. Han, C. S. Lim, Y. H. Lu, J. Wang, J. Xu, H. Y. Chen, C. Zhang, M. H. Hong, X. G. Liu, *Nature* **2010**, *463*, 1061; e) Y. F. Yang, Y. Z. Jin, H. P. He, Q. L. Wang, Y. Tu, H. M. Lu, Z. Z. Ye, *J. Am. Chem. Soc.* **2010**, *132*, 13381; f) F. V. Mikulec, M. Kuno, M. Bennati, D. A. Hall, R. G. Griffin, M. G. Bawendi, *J. Am. Chem. Soc.* **2000**, *122*, 2532; g) D. A. Chen, R. Viswanatha, G. L. Ong, R. G. Xie, M. Balasubramaninan, X. G. Peng, *J. Am. Chem. Soc.* **2009**, *131*, 9333; h) D. Q. Chen, Y. L. Yu, F. Huang, P. Huang, A. P. Yang, Y. S. Wang, *J. Am. Chem. Soc.* **2010**, *132*, 9976.

[2] a) G. F. Wang, Q. Peng, Y. D. Li, *Acc. Chem. Res.* **2011**, *44*, 322; b) J. C. G. Bünzli, *Chem. Rev.* **2010**, *110*, 2729; c) F. Wang, X. G. Liu, *Chem. Soc. Rev.* **2009**, *38*, 976; d) W. Feng, L. D. Sun, Y. W. Zhang, C. H. Yan, *Coord. Chem. Rev.* **2010**, *254*, 1038.

[3] a) F. Wang, X. J. Xue, X. G. Liu, *Angew. Chem.* **2008**, *120*, 920 – 923; *Angew. Chem. Int. Ed.* **2008**, *47*, 906 – 909; b) X. C. Ye, J. E. Collins, Y. J. Kang, J. Chen, D. T. N. Chen, A. G. Yodh, C. B. Murray, *Proc. Natl. Acad. Sci. USA* **2010**, *107*, 22430; c) S. Sivakumar, F. C. J. M. van Veggel, M. Raudsepp, *J. Am. Chem. Soc.* **2005**, *127*, 12464; d) J. C. Boyer, F. Vetrone, L. A. Cuccia, J. A. Capobianco, *J. Am. Chem. Soc.* **2006**, *128*, 7444; e) R. Si, Y. W. Zhang, L. P. You, C. H. Yan, *Angew. Chem.* **2005**, *117*, 3320; *Angew. Chem. Int. Ed.* **2005**, *44*, 3256.

[4] a) F. Zhao, M. Yuan, W. Zhang, S. Gao, *J. Am. Chem. Soc.* **2006**, *128*, 11758; b) H. S. Peng, S. H. Huang, F. T. You, J. J. Chang, S. Z. Lu, L. Cao, *J. Phys. Chem. B* **2005**, *109*, 5774; c) Q. L. Dai, H. W. Song, M. Y. Wang, X. Bai, B. Dong, R. F. Qin, X. S. Qu, H. Zhang, *J. Phys. Chem. C* **2008**, *112*, 19399; d) Z. G. Liu, X. D. Sun, S. K. Xu, J. B. Lian, X. D. Li, Z. M. Xiu, Q. Li, D. Huo, J. G. Li, *J. Phys. Chem. C* **2008**, *112*, 2353; e) J. Dhanaraj, R. Jagannathan, D. C. Trivedi, *J. Mater. Chem.* **2003**, *13*, 1778.

[5] R. G. Pearson, *J. Am. Chem. Soc.* **1963**, *85*, 3533.

[6] R. D. Shannon, *Acta Crystallogr. Sect. A* **1976**, *32*, 751.

[7] a) S. B. Zhang, J. E. Northrup, *Phys. Rev. Lett.* **1991**, *67*, 2339; b) S. H. Wei, S. B. Zhang, A. Zunger, *J. Appl. Phys.* **1999**, *85*, 7214.

[8] A. G. Dong, J. Chen, P. M. Vora, J. M. Kikkawa, C. B. Murray, *Nature* **2010**, *466*, 474.

[9] E. W. J. L. Oomen, A. M. A. Vandongen, *J. Non-Cryst. Solids* **1989**, *111*, 205.

[10] B. Henderson, G. Imbusch, *Optical Spectroscopy of Inorganic Solids*, Clarendon Press, Oxford, **1989**; p. 173.

